

RESEARCH ARTICLE | NOVEMBER 05 2024

## Forced flow reversal in ferrofluidic Couette flow via alternating magnetic field

Sebastian A. Altmeyer  



*Physics of Fluids* 36, 114105 (2024)

<https://doi.org/10.1063/5.0238005>



### Articles You May Be Interested In

Transforming underground to surface mining operation – A geotechnical perspective from case study

*AIP Conference Proceedings* (November 2021)

Monthly prediction of rainfall in nickel mine area with artificial neural network

*AIP Conference Proceedings* (November 2021)

Estimation of Karts groundwater based on geophysical methods in the Monggol Village, Saptosari District, Gunungkidul Regency

*AIP Conference Proceedings* (November 2021)



Physics of Fluids

## Special Topics Open for Submissions

[Learn More](#)



# Forced flow reversal in ferrofluidic Couette flow via alternating magnetic field

Cite as: Phys. Fluids **36**, 114105 (2024); doi: [10.1063/5.0238005](https://doi.org/10.1063/5.0238005)  
Submitted: 9 September 2024 · Accepted: 15 October 2024 ·  
Published Online: 5 November 2024



View Online



Export Citation



CrossMark

Sebastian A. Altmeyer<sup>a)</sup> 

## AFFILIATIONS

Castelldefels School of Telecom and Aerospace Engineering, Universitat Politècnica de Catalunya, 08034 Barcelona, Spain

<sup>a)</sup> Author to whom correspondence should be addressed: [sebastian.andreas.altmeyer@upc.edu](mailto:sebastian.andreas.altmeyer@upc.edu)  
and <http://www.sebastianaltmeyer.de>

## ABSTRACT

Time-dependent boundary conditions are very common in natural and industrial flows and by far no exception. An example of this is the movement of a magnetic fluid forced due to temporal modulations. In this study, we used numerical methods to examine the dynamics of ferrofluidic wavy vortex flows (WVF<sub>2</sub>, with dominant azimuthal wavenumber  $m = 2$ ) in the counter-rotating Taylor–Couette system, which was subjected to time-periodic modulation/forcing in a spatially homogeneous magnetic field. In the absence of a magnetic field, all WVF<sub>2</sub> states move in the opposite direction to the rotation of the inner cylinder, they are retrograde. However, when strength or frequency of the alternating magnetic field increases, the motion direction of the flow pattern changes. Thus, the alternating field provides a precise and controllable key parameter for triggering the system response and controlling the flow. Aside, we also observed intermittent behavior when one solution became unstable, leading to random transitions in both, the transition time and toward the different final solutions. Our findings suggest that, in ferrofluids, flow pattern reversal can be induced by varying a magnetic field in a controlled manner, which may have applications in the development of modern fluid devices in laboratory experiments. These findings provide a framework to study other types of magnetic flows driven by time-dependent forcing.

© 2024 Author(s). All article content, except where otherwise noted, is licensed under a Creative Commons Attribution-NonCommercial-NoDerivs 4.0 International (CC BY-NC-ND) license (<https://creativecommons.org/licenses/by-nc-nd/4.0/>). <https://doi.org/10.1063/5.0238005>

## I. INTRODUCTION

The observation of flow reversal upon parameter changes or perturbations is closely related to intriguing phenomena in nature, such as geomagnetic reversal. Here, the interchange of the positions between the magnetic north and south pole due to a drastic change in a planet's magnetic field<sup>1</sup> is only one example. The latter is caused by the dynamo action in which the convection of molten iron in the core produces electric currents, generating a geomagnetic field, and then the reversal of the molten iron flow direction triggers the geomagnetic field to switch the poles. Such a switch of the geomagnetic field, which typically occurs within a few 10 000 years has been investigated in several computational fluid models incorporating the interaction between electromagnetism and fluid dynamics.<sup>2–5</sup> This, among others, motivates this work to investigate the dynamical mechanism involved, in controlling and generating the flow to reverse.

In this study, we discuss the occurrence of flow pattern reversals induced by an alternating magnetic field in the classic Taylor–Couette system (TCS).<sup>6</sup> The TCS [Fig. 1(a)] is a well-known hydrodynamic system that has been extensively studied through experiments,

analysis, and computational methods, and is crucial for understanding fundamental fluid dynamics phenomena for many decades.<sup>7–11</sup> While time-periodic forcing in TCS with classical Newtonian fluid has been explored in earlier works,<sup>12–17</sup> it has been introduced into the system through modifications of boundary conditions, such as axial or azimuthal oscillation of cylinders, pulsation of axial imposed flow, or radial through flow (requiring porous cylinder walls). By considering magnetic fluids like ferrofluids,<sup>18</sup> we can directly realize periodic forcing within the fluid in the annulus without altering the original boundary conditions. Such magnetic nanofluids have a wide range of applications, from embedded fluidic devices in computer hard drives to laboratory experiments exploring the fundamentals of geophysical flows,<sup>19,20</sup> and eventually, aerospace applications.<sup>21,22</sup>

Ferrofluids were first developed in 1963 by NASA scientist Stephen Papell as a potential rocket fuel. These fluids contain tiny magnetized particles at the nanoscale. In the absence of an external magnetic field, the fluid has zero net magnetization because the magnetic moments of the nanoparticles are randomly oriented. In this state, the influence of the magnetized particles on the physical

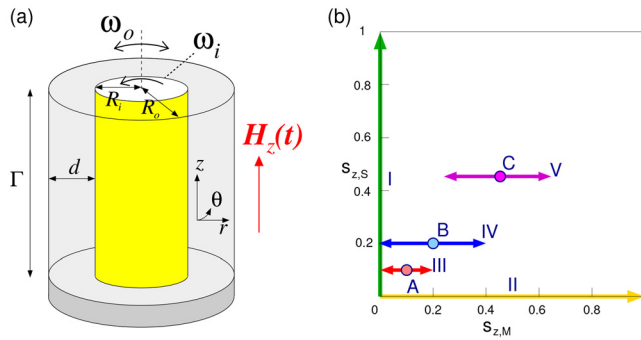


**FIG. 1.** System and explored parameter space. (a) Geometry of the Taylor–Couette system (TCS) (only the bottom lid serving as one of the axial end walls is indicated) with an external applied homogeneous axial magnetic field  $H_z(t) = [H_{z,S} + H_{z,M} \sin(\Omega_H t)]\mathbf{e}_z$ . (b) Parameter space: arrows I and II indicate the investigated parameter space spanned by  $s_{z,S} \in [0, 1]$  and  $s_{z,M} \in [0, 1]$ , respectively. Points A, B, and C give the parameters for different WVF<sub>2</sub> at static fields and arrows III, IV, and IV give the corresponding modulation amplitudes to this set of parameters.

properties of the fluid, such as its density and viscosity, is negligible. However, when an external magnetic field is present, the flow and dynamics of the fluid can be significantly altered. These effects range from simple shifts in solution bifurcation thresholds and changes in system stability<sup>23–27</sup> to the formation of entirely new flow structures.<sup>24,29–31</sup> Nonetheless, research on ferrofluids under alternating magnetic fields is relatively scarce, with most studies focusing on viscous effects and heat behavior.<sup>41–43</sup>

The previous research in TCS using classical fluids has revealed that the reversal of flow pattern propagation is intrinsic to the system. This was observed in simulations with both periodic boundary conditions and a finite length annulus (closed lids on both sides), which resulted in similar wave propagation reversal.<sup>40</sup> Furthermore, in ferrofluidic Taylor–Couette flow under periodic boundary conditions, wave propagation reversal can be induced by modifying a static magnetic field,<sup>35</sup> while maintaining the same azimuthal wavenumber.

Our study focuses on the effects of an alternating magnetic field with variations in modulation amplitude and frequency on the flow dynamics. We analyze how the modification in the azimuthal wave speed ( $\omega$ ) of the wavy instability leads to it reaching zero and eventually changing its sign, causing the waves to move in the opposite direction. For the considered parameters of constant and sufficiently large counter-rotation, the wavy flow transitions from retrograde to prograde behavior as the magnetic field modulation is increased. Additionally, we describe the complex flow dynamics that emerge for such alternating field parameters when the system is at the edge between prograde and retrograde dynamics, resulting in an oscillating standing wave. In this context, with modulation in the driving frequency, we also observed intermittency dynamics.

The outline of the paper is as follows. Following the introduction, Sec. II describes the basic equations, numerical method as well as the explored parameter space. Thereafter, Sec. III presents the numerical results starting with an introduction to the WVF state that is considered. This is followed by an investigation of the bifurcation scenario via static and alternating magnetic fields together with an analyze in flow dynamics and spatial-temporal characteristics that coincides with

the wave propagation reversal, in particular with respect to driving frequency  $\Omega_H$ . Finally, Sec. IV provides a discussion and conclusions.

## II. MATERIALS AND METHODS

### A. Governing equations

For this work, the radius ratio is fixed to 0.5 (wide gap), the aspect ratio to  $\Gamma = 10$  while varying the axial alternating magnetic field. Further, the inner and outer cylinders (of radii  $R_i$  and  $R_o$ ) are held at constant rotation speed corresponding to inner and outer Reynolds numbers  $Re_i = 300$  and  $Re_o = -145$  ( $Re_{i|o|} = \omega_{i|o|} r_{i|o|} d / \nu$  is the ratio between inertia and viscous forces,  $\nu$  is the kinematic viscosity). Further, non-rotating fixed endplates are considered, which resulted in no-slip-fixed rigid boundary conditions (RBC) with zero velocity at  $z = \pm \Gamma/2$ . The latter breaks the  $O(2)$  axial symmetry of the (infinite) periodic TCS. The boundary conditions are  $u(r_i, \theta, z, t) = (0, Re_i, 0)$ ,  $u(r_o, \theta, z, t) = (0, Re_o, 0)$ , and  $u(r, \theta, \pm \Gamma/2, t) = (0, 0, 0)$ , where the non-dimensional inner and outer radii are  $r_i = R_i/d$  and  $r_o = R_o/d$ , with gap  $d = r_o - r_i$ . The gap between the cylinders is filled with a viscous, incompressible, isothermal magnetic based ferrofluid APG933.<sup>33,34</sup>

We realize the periodic forcing in the system via a sinusoidal modulation signal to the external magnetic field, which is orientated parallel to the system symmetry ( $z$ ) axis, uniform in space, and harmonic in time<sup>27,28</sup>

$$\mathbf{H}_z = [H_S + H_M \sin(\Omega_H t)]\mathbf{e}_z. \quad (1)$$

It is important mentioning that such a *pure* axial-oriented magnetic field does *not* change the basic system symmetry, only the stability thresholds are altered.<sup>23–25</sup>

The flow dynamics of a ferrofluid are governed by the incompressible Navier–Stokes equations, including additional magnetic terms, and the continuity equation. Using the gap width  $d$  as the length scale, the diffusion time  $\tau_D = d^2/\nu$  as the timescale, scaling pressure with  $\rho\nu^2/d^2$ , and the magnetic field  $\mathbf{H}$  and the magnetization  $\mathbf{M}$  with  $(\rho/\mu_0)^{0.5}\nu/d$  ( $\mu_0$  is the magnetic constant, which is the magnetic permeability of free space), the non-dimensionalized ferro-hydrodynamical equations of motion and continuity equation<sup>26,27,29,36</sup> read

$$(\partial_t + \mathbf{u} \cdot \nabla)\mathbf{u} - \nabla^2 \mathbf{u} + \nabla p = (\mathbf{M} \cdot \nabla)\mathbf{H} + \frac{1}{2} \nabla \times (\mathbf{M} \times \mathbf{H}), \quad (2)$$

$$\nabla \cdot \mathbf{u} = 0.$$

Equation (2) is solved together with an equation that describes the magnetization of the ferrofluid. Here we consider the equilibrium magnetization of an unperturbed state, in which a homogeneously magnetized ferrofluid is at rest. Under this condition, the mean magnetic moments are orientated in the direction of the magnetic field and one finds  $M_{eq} = \chi H$ . Further, we use the Langevin formula, with an assumed initial value 0.9 and approximately a linear magnetization law in order to determine approximately the magnetic susceptibility  $\chi$  of the ferrofluid. In addition, the near equilibrium approximations of Niklas<sup>23</sup> is considered, with small deviations  $\|M - M_{eq}\|$  and small magnetic relaxation time  $\tau: |\nabla \times u|, \tau \ll 1$ . A more detailed description of the numerical procedure and elimination process can be found in the Appendix of an earlier work.<sup>27</sup>

The biggest advantage in using such a modified Niklas approach<sup>23,24,27,29</sup> is the fact that all the effects of the magnetic field and the magnetic properties of the ferrofluid on the velocity field can be characterized by a single (time-dependent) parameter/function:

$$s_z(t) = s_{z,S} + s_{z,M} \sin(\Omega_H t), \tag{3}$$

with  $s_{z,S}$  being the static contribution,  $s_{z,M}$  being the modulation amplitude, and  $\Omega_H$  being the modulation frequency. For the exact procedure and more details of how to solve the ferro-hydrodynamical equations of motion [Eq. (2)], we refer to our earlier works.<sup>26–29</sup>

### B. Symmetries

TCS is invariant under different spatiotemporal operations. The governing equations and the boundary conditions are invariant under arbitrary rotations  $R_x$  about the axis, reflections  $K_z$  about the annulus mid-plane  $z = 0$ , and with respect to time translations  $\Phi_{t_0}$ , generating the symmetry group  $SO(2) \times Z_2 \times \mathbb{R}$ . Thereby, the first two factors consist of the purely spatial symmetries, and the third factor corresponds to the temporal symmetries generating the one-dimensional translation group  $R$ . The actions of the three symmetries on the velocity field are

$$R_x(u, v, w)(r, \theta, z, t) = (u, v, w)(r, \theta + \alpha, z, t), \tag{4a}$$

$$K_z(u, v, w)(r, \theta, z, t) = (u, v, -w)(r, \theta, -z, t), \tag{4b}$$

$$\phi_{t_0}(u, v, w)(r, \theta, z, t) = (u, v, w)(r, \theta, z, t + t_0). \tag{4c}$$

### C. Numerical method

The ferro-hydrodynamic equations [Eq. (2)] are solved using a second-order time-splitting method with consistent boundary conditions for the pressure.<sup>37,38</sup> Our code G1D3<sup>24,39</sup> is a combination of a finite-difference method in the radial and axial directions ( $r, z$ ) and a Fourier–Galerkin expansion in the azimuthal direction ( $\theta$ ) with time splitting, which leads to the following decomposition:

$$f(r, \theta, z, t) = \sum_m f_m(r, z, t) e^{im\theta} \tag{5}$$

for all fields  $f \in \{u, v, w, p\}$ .

In order to characterize the different flow structures, we consider different quantities. First, as a global measure of the flow, we use the total modal kinetic energy:

$$E_{kin} = \sum_m E_m = \frac{1}{2} \int_0^{2\pi} \int_0^z \int_{r_i}^{r_o} \mathbf{u}_m \mathbf{u}_m^* r dr dz d\theta, \tag{6}$$

where  $\mathbf{u}_m$  ( $\mathbf{u}_m^*$ ) is the  $m$ th (complex conjugate) Fourier mode [Eq. (5)] of the velocity field. For instance, in the case of an axisymmetric solutions ( $m = 0$ ) – here CCF and TVF, only  $E_0$  is non-zero. Second, as a measure more closely related to the vortices and corresponding azimuthal and axial wavenumbers, we utilize the azimuthal decomposition [Eq. (5)] of the radial velocity field. Therefore, we perform an additional axial Fourier analysis of the mode amplitudes  $u_m(z, t)$  at mid-gap,  $r = r_1 + d/2$ . We then identify for the dominant azimuthal wavenumber, here  $m = 2$ , the largest contribution in the axial Fourier spectrum of  $u_m(z, t)$  for the patterns with  $k = 4.21$ ,  $k = 3.85$ , and  $k = 3.69$ . It is worth mentioning that these wavenumbers  $k$  are not externally forced, they are natural selected by the system based on system parameters such as aspect ratio, radius ratio, and Reynolds numbers. The oscillation of the corresponding complex Fourier amplitudes describes the frequencies  $\omega_{m,k}$ . It is this quantity that describes the wavy instability, and a change in its sign is direct correlated with the

wave propagation reversal. We identify the specific flow structures by the abbreviation  $(m, k)$ . These modes reflect the symmetry properties of the vortex structures. Thus, the Fourier spectrum of the TVF solution contains the two dominant modes  $(0, [-]k)$ , with one being the complex conjugate. The spectrum of wavy vortex flow with two waves corresponding to azimuthal wavenumber  $m = 2$  (hereafter designated as  $WVF_2$ ) is dominated by  $(2, k)$  and its complex conjugate  $(-2, -k)$  as well as the still dominant axisymmetric components  $(0, k)$  and  $(0, -k)$ . This  $WVF_2$  appears also with different number of vortex pairs within the annulus. Here we focus on  $WVF_2$  with either five vortex pairs [ $WVF_2(k = 4.21)$ ] or four vortex pairs [ $WVF_2(k = 3.85)$ ,  $WVF_2(k = 3.69)$ ] in the bulk (in addition to the Ekman vortices close to the lids). For visualization purposes, we consider the azimuthal vorticity component,  $\eta = (\nabla \times u) \cdot e_\theta = \partial_z u - \partial_r w$ , as an adequate and convenient measure to identify and recognize the geometry of complex vortex structures via iso-vorticity surfaces.<sup>32</sup> Further, we also use the global mean angular velocity  $V_\pm = \langle v/r \rangle_{r,\theta,z}$  (nondimensionalized by the inner cylinder rotation  $\omega_i$ ), which can be different from the azimuthal wave speed  $\omega_{m,k}$  reflecting the wavy instability. However, the sign of  $\omega_{m,k}$  determines the direction of wave propagation [positive (+) for prograde and negative (–) for retrograde with respect to the rotation direction of the inner cylinder].

### D. System – parameters setting and quantities

We explore the parameter space for static contribution  $s_{z,S} \in [0, 1]$ , modulation amplitude  $s_{z,M} \in [0, 1]$ , and forcing frequency  $\Omega_H \in [0.1, 500]$ . Trajectories I and II shown in the parameter space of Fig. 1 represent pure static and pure alternating magnetic fields, respectively. Points A, B, and C corresponding to parameters for different  $WVF_2$  with the trajectories III, IV, and V highlight the parameters at which we provide a more detailed study for alternating magnetic field [cf. Fig. 2(1c)].

## III. RESULTS

### A. Wavy flow states

In TCS, the relative speed of rotation of the inner and outer cylinders defines the rotational direction of the flow pattern. A most common scenario in the absence of any magnetic field is that the flow pattern follows the rotational direction of the inner cylinder, which is commonly referred to as the “normal” scenario – the flow is prograde. However, for strong counter-rotations of both cylinders and some other critical parameters, the flow pattern may follow the rotational direction of the outer cylinder.<sup>39</sup> The latter also applies to here chosen system parameters. In the absence of any magnetic field, both wavy flows  $WVF_2(5V, k = 4.21)$  and  $WVF_2(4V, k = 3.69)$  are retrograde in the sense that they rotate against the rotational direction of the inner cylinder.

Before discussing any complex dynamics forced due to an alternating magnetic field, we briefly describe the different wavy flow patterns that can occur for the range of parameters that we consider: wavy flows  $WVF_2(5V, k = 4.21)$ ,  $WVF_2(4V, k = 3.85)$ , and  $WVF_2(4V, k = 3.69)$ , which all have  $m = 2$  twofold azimuthal periodicity, as illustrated in Fig. 3. We also detected other wavy flows with threefold symmetry ( $WVF_3$ ), but they are not further interesting for the current study. The different states can exist with prograde or retrograde characteristics.

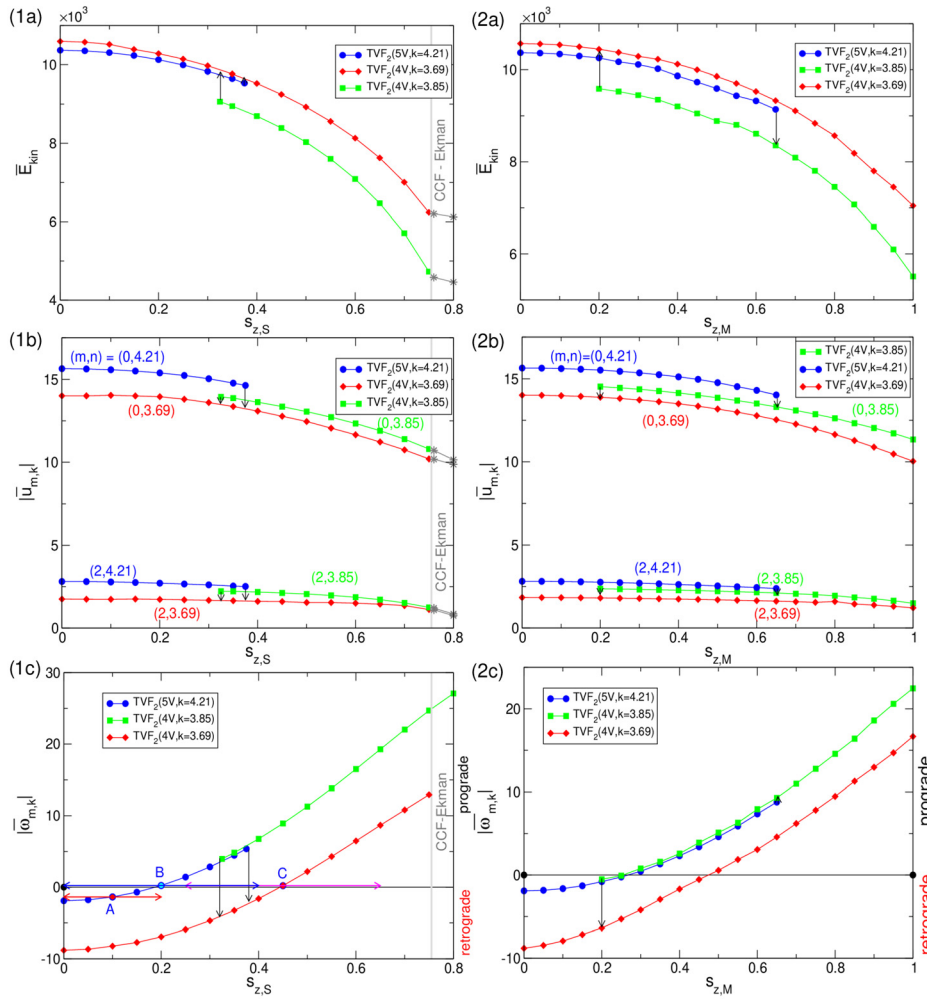


**FIG. 2.** Bifurcation behavior with (1)  $s_{z,S}$  and (2)  $s_{z,M}$ . Variation with  $s_{z,S}$  [ $s_{z,M}$ ] of (a) (time-averaged) the modal kinetic energy  $\bar{E}_{kin}$  [Eq. (6)], (b) (time averaged) moduli  $|\bar{u}_{m,k}|$  of the dominant axial Fourier amplitudes of the azimuthal modes  $u_m(z, t)$  [Eq. (5)] of the radial flow at mid-gap, and (c) the corresponding frequencies,  $\omega_{m,k}$  for the flow states,  $WVF_2(5V, k = 4.21)$ ,  $WVF_2(4V, k = 3.69)$ , and  $WVF_2(4V, k = 3.85)$ . Symbols primarily distinguish different structures, but do not represent the resolution of the calculations, which varies depending on the proximity with respect to the wave propagation reversal; vertical arrows indicate the transition toward a new solution if the old one becomes unstable. Horizontal arrows with labels A, B, and C in (1c) (see also Fig. 1) highlight parameters for which frequency dependence will be studied later.

The contours of the radial velocity  $u(\theta, z)$  on an unrolled cylindrical surface at mid-gap [Fig. 3(a)], as well as the contours of the azimuthal velocity component  $v$  in the  $(r, \theta)$  plane at mid-height [Fig. 3(e)], clearly show the azimuthal  $m = 2$  symmetry of these states.

Moreover, the isosurfaces of azimuthal vorticity [Fig. 3(b)]  $\eta$  provide an impression of the flow structures of these wavy states. For the selected field strength  $s_{z,S} = 0.35$ , all wavy flows are stable and coexisting.  $WVF_2(5V, k = 4.21)$  and  $WVF_2(4V, k = 3.85)$  exhibit prograde wave propagation, meaning the waves follow the inner cylinder rotation. On the other hand,  $WVF_2(4V, k = 3.69)$  moves in the opposite direction, indicating retrograde behavior, as indicated by the arrows below the images.

The different wavy states vary in the sense that they have different axial wave numbers  $k$  (wavelengths  $\lambda$ ) due to different numbers of vortex pairs in the annulus.  $WVF_2(5V, k = 4.21)$  has five vortex pairs (plus two Ekman cells), resulting in an axial wave number  $k = 4.21$  ( $k = 1.49$ ). Meanwhile,  $WVF_2(4V, k = 3.85)$  and  $WVF_2(4V, k = 3.69)$  each have one vortex pair less (in total 4, plus two Ekman cells) within the bulk. However, for the latter, the Ekman cells near the

lids have different sizes, resulting in different axial wavenumbers  $k = 3.85$  ( $\lambda = 1.63$ ) and  $k = 3.69$  ( $\lambda = 1.70$ ), respectively.

In the following, we will analyze what happens if a magnetic field is present.

## B. Static magnetic field ( $s_{z,M} = 0$ )

Figure 2(1) illustrates the evolution of the different  $WVF_2$  solutions (Fig. 3) under the presence of pure axial, static magnetic field  $s_{z,S}$ . To characterize the flow structures, we examine kinetic energy  $E_{kin}$ , radial flow field amplitudes  $|u_{m,k}|$  at mid-gap (time-averaged for time-dependent solutions), and corresponding frequencies  $\omega_{m,k}$  of the dominant axial Fourier amplitudes  $u_m(z, t)$  [Eq. (5)]. In the case of the radial flow field amplitudes, we display the contributions of the dominant, axisymmetric ( $m = 0$ ) mode, as well as the dominant non-axisymmetric ( $m = 2$ ) mode embedded in the solution and characterizing the wavy solution. In the absence of a magnetic field, the two solutions  $WVF_2(5V, k = 4.21)$  and  $WVF_2(4V, k = 3.69)$  are bistable coexisting. With increasing axial field strength  $s_{z,S}$ , the kinetic energy

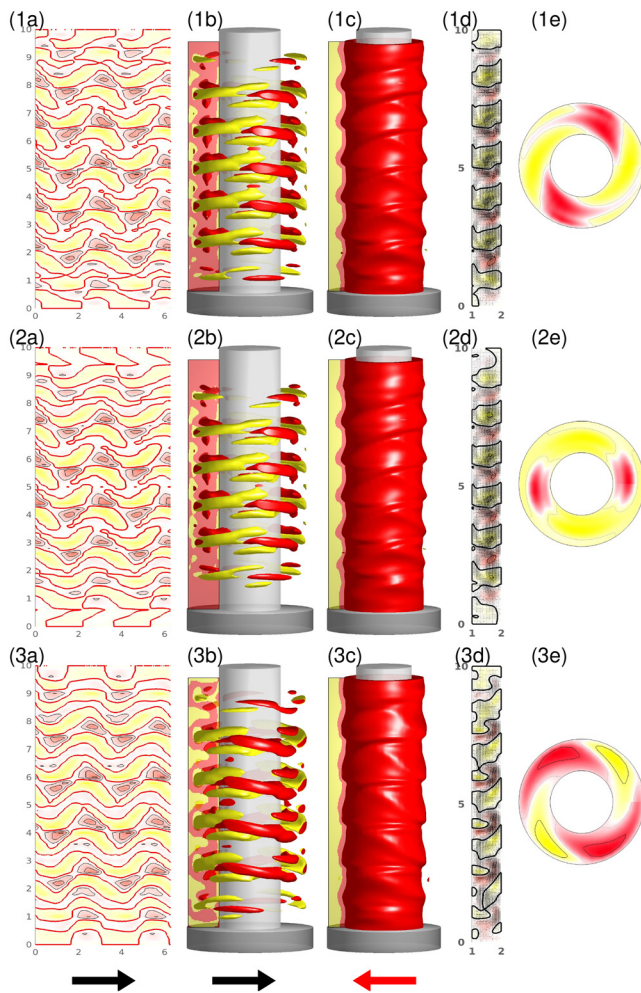


**FIG. 3.** Flow visualizations of different stable  $WVF_2$  states at  $s_{z,S} = 0.35$  ( $s_{z,M} = 0$ ). (1)  $WVF_2(5V, k = 4.21, t)$ , (2)  $WVF_2(4V, k = 3.85, t)$ , and (3)  $WVF_2(4V, k = 3.69)$ ,  $WVF_2(5V, k = 4.21)$ , and  $WVF_2(4V, k = 3.85)$  are prograde in the sense of following the inner cylinder rotation (see arrows below the images), while  $WVF_2(4V, k = 3.69)$  is retrograde, with the flow pattern *not* following the inner cylinder rotation. Shown are (a) radial velocity  $u(r, z)$  on an unrolled cylindrical surface in the annulus at mid-gap [red (yellow) color indicates in (out) flow], (b) isosurfaces of azimuthal vorticity  $\eta = (\nabla \times \mathbf{u}) \cdot \mathbf{e}_\theta = \partial_z u - \partial_r w = \pm 200$  [red (yellow) color indicates positive (negative) vorticity], (c) isosurface of azimuthal velocity after subtracting the local azimuthal velocity for circular Couette flow,  $v - v_{CCF}$ , (d) vector plot  $[u(r, z), w(r, z)]$  of the radial and axial velocity components (including the color-coded azimuthal velocity  $v$ ), and (e) the azimuthal velocity component  $v$  in  $(r, \theta)$  plane at mid-height (viewed from the bottom) [red (yellow) color indicates positive (negative) velocity]. Note that both  $WVF_2(5V, k = 4.21, t)$  and  $WVF_2(4V, k = 3.85, t)$  are time-dependent states.

and all mode amplitudes for any shown solution  $WVF_2$  decrease monotonically [Figs. 2(1a) and 2(1b)]. This is a result of the well-known effect that any applied magnetic field stabilizes the basic state<sup>24</sup> and thus the decrease in kinetic energy and particular mode amplitudes indicates the shift closer to the bifurcation onset. The  $WVF_2(4V, k = 3.69)$  remains stable until disappearing at its bifurcation onset at  $s_{z,S} \approx 0.76$ , hereafter only the CCF-Ekman state<sup>39</sup> is

present. On the other hand,  $WVF_2(5V, k = 4.21)$  becomes unstable with increasing field strength at  $s_{z,S} \approx 0.37$  at which point it transitions to the stable  $WVF_2(4V, k = 3.69)$  solution (indicated by vertical arrow). Meanwhile for larger  $s_{z,S}$ , we detected the  $WVF_2(4V, k = 3.85)$  solution. It bifurcates stable out of the CCF-Ekman basic state but loses its stability with decreasing  $s_{z,S}$  and transitions at  $s_{z,S} \approx 0.32$  to the stable branch of  $WVF_2(4V, k = 3.69)$ . It is worth mentioning that we never saw a transition to the  $WVF_2(5V, k = 4.21)$  solution with a larger number of vortices in the axial direction.

The kinetic energy  $E_{kin}$  for the two solutions  $WVF_2(5V, k = 4.21)$  and  $WVF_2(4V, k = 3.69)$  is very similar, as shown in Fig. 2(1a). This similarity can be understood because the system finds it easier to adjust the axial wavenumber rather than to generate another vortex pair within the annulus. When examining the corresponding frequencies [Fig. 2(1c)] of the complex mode amplitudes (correlated with the rotation direction of the whole flow structure), one can observe a monotonically increasing  $\omega$  with increasing field strength  $s_{z,S}$ . For  $s_{z,S} = 0$ , both flow states,  $WVF_2(5V, k = 4.21)$  and  $WVF_2(4V, k = 3.69)$ , are retrograde ( $\omega < 0$ ). However, the corresponding frequencies increase, cross zero, and become positive at  $s_{z,S} \approx 0.19$  for  $WVF_2(5V, k = 4.21)$  and at  $s_{z,S} \approx 0.489$  for  $WVF_2(4V, k = 3.69)$ . After this point, the entire flow pattern is now prograde.  $WVF_2(4V, k = 3.85)$  does not show any flow pattern reversal and only exists stably as a solution with prograde dynamics.

### C. Alternating magnetic field ( $s_{z,M} \neq 0$ )

Increasing the modulation amplitude  $s_{z,M}$  has a stabilizing effect on the system, leading to a decrease in kinetic energy  $E_{kin}$  and mode amplitudes  $|u_{m,k}|$  [Fig. 2(2)]. This effect is similar to increasing the field strength  $s_{z,S}$  in the static case, but it is quantitatively weaker. With the maximum modulation amplitude considered here,  $s_{z,M} = 1$ , the system does not reach the bifurcation point of the respective solution and therefore does not enter the CCF-Ekman basic state. Just like in the static scenario, the flow state  $WVF_2(4V, k = 3.69)$  remains stable throughout the investigated parameter range, while  $WVF_2(5V, k = 4.21)$  loses stability and transitions toward  $WVF_2(4V, k = 3.85)$  at  $s_{z,M} \approx 0.65$ .  $WVF_2(4V, k = 3.85)$  is only stable for sufficiently large  $s_{z,M}$  and loses stability at smaller values,  $s_{z,M} \approx 0.2$ , against the  $WVF_2(4V, k = 3.69)$  flow state (as indicated by vertical arrows in Fig. 2). As the field amplitude  $s_{z,M}$  increases, the corresponding frequencies  $\Omega_H$  [Fig. 2(c)] also monotonically increase, cross zero, and eventually become positive, signifying a change from retrograde to prograde characteristics. Interestingly,  $WVF_2(4V, k = 3.85)$  also crosses zero and changes its flow direction to prograde, whereas for static magnetic field, it is only stable with prograde dynamics. The modulation amplitudes for the zero crossings are very close to each other (but not identical) for  $WVF_2(5V, k = 4.21)$  at  $s_{z,M} \approx 0.27$  and  $WVF_2(4V, k = 3.85)$  at  $s_{z,M} \approx 0.26$ . At larger values,  $s_{z,M} \approx 0.47$ ,  $WVF_2(4V, k = 3.69)$  eventually changes from retrograde to prograde.

### D. Frequency dependence ( $\Omega_H$ )

Next, we will take a closer look at the non-linear dynamics as the oscillation frequency varies. To do this, we will analyze the system response for two different sets of parameters: (1) small modulation amplitude, where  $s_{z,S} = 0.1 = s_{z,M}$  (point A in Figs. 1 and 2), and

(2) large modulation amplitude, where  $s_{z,S} = 0.2 = s_{z,M}$  (points B and C in Figs. 1 and 2).

### 1. Small modulation amplitude ( $s_{z,S} = 0.1 = s_{z,M}$ )

Figure 4 shows the oscillation of the control function  $s_z(t)$  together with the system response. It illustrates the mode amplitudes  $|u_{2,4.21}|$  and corresponding frequency  $|\omega_{2,4.21}|$  for  $WVF_2(5V, k = 4.21)$  and  $|u_{2,3.85}|$  with  $|\omega_{2,3.85}|$  for  $WVF_2(4V, k = 3.85)$ . This is shown as a function of the reduced time  $t/T_H$  ( $T_H = 2\pi/\Omega_H$  representing the associated modulation period of the alternating field). Temporal oscillations are depicted for different frequencies  $\Omega_H$  as indicated. In the high-frequency limit, mainly the time average of  $s_z(t)$

affects the flow dynamics and stability behavior. In this case, the equivalent static magnetic Niklas parameter is larger than the mean value  $\langle s_z(t) \rangle_T$ , which is indicated by the horizontal dashed line in Fig. 4.

In the high-frequency limit ( $\Omega_H = 500$ ), for  $WVF_2(5V, k = 4.21)$ , the variations in the dominant mode amplitude  $|u_{2,4.21}|$  are small compared to its mean value. However, they are slightly bigger in  $|u_{2,3.85}|$  for  $WVF_2(4V, k = 3.85)$  [Figs. 4(b) and 4(c)]. In both cases, a phase shift occurs between the maximum and minimum of the field function  $s_z(t)$  and between the minimum and maximum of the mode amplitudes  $|u_{2,4.21}|$ ,  $|u_{2,3.85}|$ . This phase shift is caused by the fluid's inertia resisting the fast-changing accelerating Kelvin force, resulting in a temporal delay. As the frequency decreases, the phase shift also decreases, while the oscillation amplitudes increase. For low

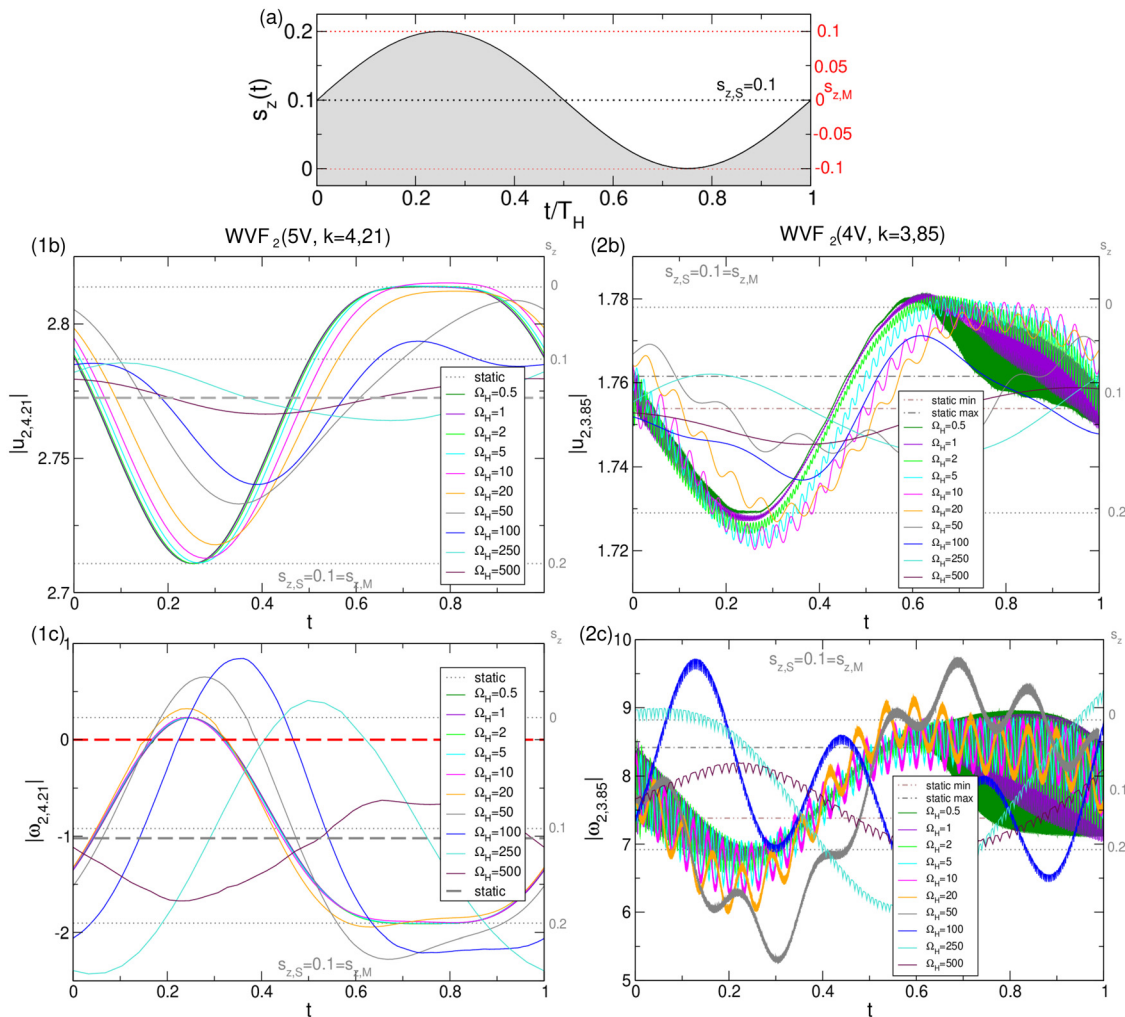


**FIG. 4.**  $WVF_2$  under alternating axial magnetic field  $s_z(t)$  with different driving frequencies  $\Omega_H$  for flow structures (1)  $WVF_2(5V, k = 4.21)$  and (2)  $WVF_2(4V, k = 3.85)$ . (a) Temporal oscillations of the control function  $s_z(t) = s_{z,S} + s_{z,M} \sin(\Omega_H t)$  [Eq. (3)]. Shown are the dominant (a, b) mode amplitude and frequency  $|u_{2,4.21}|$ ,  $|\omega_{2,4.21}|$   $WVF_2(5V, k = 4.21)$  and  $|u_{2,3.85}|$ ,  $|\omega_{2,3.85}|$  for  $WVF_2(4V, k = 3.85)$  as a function of the reduced time  $t/T_H$  ( $T_H = 2\pi/\Omega_H$  being the modulation period associated with the corresponding frequency) for parameter values  $s_{z,S} = 0.1 = s_{z,M}$  are displayed. Horizontal gray dotted lines indicate the static limits for  $s_{z,S} = 0, 0.1$ , and  $0.2$ , respectively, while the horizontal gray dashed line gives the high frequency limit. The horizontal red dotted line in (1c) highlights the zero-crossing as characterization for retrograde and prograde dynamics, respectively. Note, that the  $WVF_2(4V, k = 3.85)$  (2) is already a time-dependent solution in the absence of any field. Thus, here the horizontal dotted lines only illustrate the corresponding time-averaged values for  $s_{z,S} = 0, 0.1$ , and  $0.2$ , respectively.

modulation frequency, the oscillation profiles approach the curve of a static magnetic field, which is asymmetric due to a larger stabilization effect for positive modulation amplitude in comparison to the destabilization effect for the same but negative modulation amplitude.

The behavior of  $WVF_2(4V, k = 3.85)$  [Fig. 4(2)] in a static magnetic field with  $s_{z,S} = 0.1$  and  $s_{z,M} = 0$  is time-dependent, and its oscillations appear more complex due to the natural frequency ( $\omega[WVF_2(4V, k = 3.85)] \approx 0.12$ ) of the flow. However, it exhibits qualitatively similar behavior and response as  $WVF_2(5V, k = 4.21)$ . The dynamics seem to become simpler with increasing driving frequency  $\Omega_H$ . At low frequencies  $\Omega_H$ , an overshoot in the mode amplitudes  $|u_{2,4,21}|$  and  $|u_{2,3,69}|$  is observed when approaching the static state, along with more pronounced overshoots in the corresponding frequencies  $|\Omega_{2,4,21}|$  and  $|\Omega_{2,3,69}|$  [Fig. 4(1)]. This overshoot is caused by the inertia of the fluid. The sign of the frequency of the wavy instability  $\omega_{2,4,21}$  identifies the flow as prograde (positive sign) or retrograde (negative sign). For small and moderate frequencies  $\Omega_H \lesssim 300$ ,  $\omega_{2,4,21}$  is mainly negative, changing its sign within one period of driving  $T_H$ , which corresponds to alternating retrograde and prograde dynamics [Fig. 4(1c)]. However, for driving frequencies  $\Omega_H \gtrsim 300$ , the flow remains retrograde as the wavy instability frequency  $\omega_{2,4,21}$  is always negative. Consequently, the flow/global angular velocity remains one-directional, only temporally slowing down without changing its propagation direction.

As seen before [Fig. 4(1c)], when the driving frequency  $\Omega_H$  is low,  $\Omega_H \gtrsim 300$ , the wavy instability frequency  $\omega_{2,4,21}$  changes sign within one oscillation period, causing the flow to switch between retrograde and prograde dynamics. Figure 5 illustrates the time evolution of the flow dynamics for  $WVF_2(5V, k = 4.21)$  under an alternating magnetic field with  $s_{z,S} = 0.1 = s_{z,M}$  at a driving frequency of  $\Omega_H = 5$ . In the close-up of two periods [Fig. 5(b)], you can see the system transitioning from retrograde (region A, indicated by the red left arrow) to prograde behavior (region B, indicated by the black right arrow) and vice versa when  $\omega_{2,4,21}$  crosses through zero. The brief retrograde dynamics is displayed in the  $(\eta_-, \eta_+)$  phase space as a small loop [see close-up inset in Fig. 5(c)]. It is important to note that for the parameters chosen here, it takes approximately nine periods  $T_H$  of the alternated forcing before the system returns close to its initial values in phase space [compare points 0 and 9 in Fig. 5(c)]. Therefore, from a dynamical perspective, we have a limit cycle solution  $lc$  with a small drift.

The flow visualizations in Fig. 6 [top row (multimedia online), middle row (multimedia online), and bottom row (multimedia online)] show the reversal of the temporal flow pattern for  $WVF_2$  at 5V with  $k = 4.21$ , transitioning from retrograde ( $\omega < 0$ ) to prograde ( $\omega > 0$ ) and vice versa. The visuals for different times  $t_i, i \in \{1; 5\}$  [as per Fig. 5(b)] are displayed. This correlates with the small loops visible in the  $(\eta_-, \eta_+)$  phase space [Fig. 5(c)], effectively illustrating the dynamics of the system.

The flow transitions are detailed as follows: At time  $t_1$  (region A), the flow moves rapidly with retrograde dynamics, maintaining this direction at time  $t_2$ , albeit at a significantly reduced speed, before reversing direction at time  $t_3$ . The flow with prograde dynamics at  $t_3$  is notably slow and short-lived (region B). Subsequently, the flow returns to retrograde dynamics (region A), starting slowly at  $t_4$  and gradually increasing in speed until the end of the oscillation period at  $t_5$  (which mirrors  $t_1$ ).

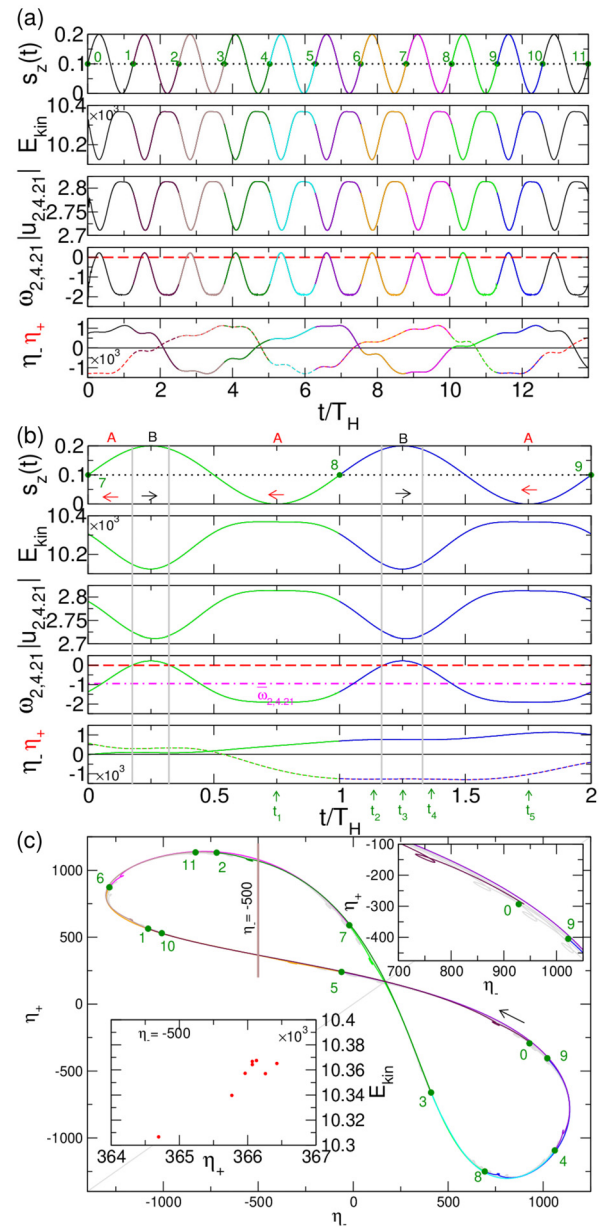


**FIG. 5.** Flow dynamics evolving with time  $t$  for  $WVF_2(5V, k = 4.21)$  for an alternating magnetic field with  $s_{z,S} = 0.1 = s_{z,M}$  and  $\Omega_H = 5$ . Shown are (a) variation with time (for 11 field oscillation periods  $T_H$ ) of the magnetic field  $s_z(t)$ , the modal kinetic energy  $E_{kin}$  [Eq. (6)], moduli  $|u_{m,k}|$  of the dominant axial Fourier amplitudes of the azimuthal modes  $u_m(z, t)$  [Eq. (5)] of the radial flow at mid-gap, and the corresponding frequencies  $\omega_{m,k}$ . (b) Close up of (a) covering two periods. The flow is retrograde in region A and prograde in region B. Small arrows below the abscissa in (b) indicate time steps  $t_i, i \in \{1; 5\}$  for which snapshots are shown in Fig. 9. Red dashed line indicates  $\omega_{2,4,21} = 0$ , while magenta dot-dashed line indicates the mean value  $\bar{\omega}_{2,4,21} = -0.95$ . (c) Phase portraits in  $(\eta_-, \eta_+) = (\eta(r = r_i, \theta = 0, z = \Gamma/4), \eta(r = r_i, \theta = 0, z = 3\Gamma/4))$  plane; inset bottom left shows the Poincaré section for  $\eta_- = -500$  (see vertical brown line) and inset top right is a close up in phase space around 0. Each oscillation period  $T_H$  is coded by a different color and the same color code is used for each subplot. The gray colored line in (c) indicates the diagonal  $\eta_+ = \eta_-$ .

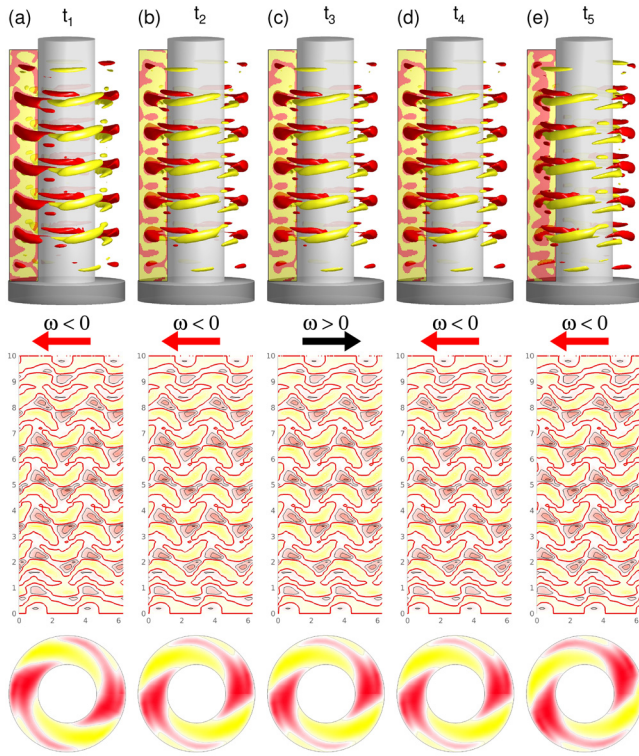


**FIG. 6.** Flow visualizations of the temporal flow pattern reversal for WVF<sub>2</sub> (5V,  $k = 4.21$ ) with  $s_{z,S} = 0.1 = s_{z,M}$  and  $\Omega_H = 5$  for retrograde ( $\omega < 0$ ) (a), (b), (d), and (e) and prograde ( $\omega > 0$ ) (c) situations at times  $t_i, i \in \{1; 5\}$  as indicated in Fig. 5. Top row: isosurfaces of azimuthal vorticity  $\eta = \pm 200$  [red (yellow) color indicates positive (negative) vorticity]. Middle row: radial velocity  $u(\theta, z)$  on an unrolled cylindrical surface in the annulus at mid-gap [red (yellow) color indicates in (out) flow]. Bottom row: contours of azimuthal velocity component  $v$  in the  $(r, \theta)$  plane at mid-height (viewed from the bottom) [red (yellow) color indicates positive (negative) velocity]. Multimedia files show two periods,  $T_\Omega \approx 1.257$ , of the alternating field. Multimedia available online.

Despite the momentary prograde behavior, the overall flow dynamics remain retrograde, as evidenced by the average value  $\overline{\omega}_{2,4,21} = -0.95$  (Fig. 6, multimedia online).

**2. Large modulation amplitude ( $s_{z,S} = 0.2 = s_{z,M}$ )**

Figure 7 illustrates the system response with variation in driving frequency  $\Omega_H$  similar to Fig. 4 but with larger modulation amplitude  $s_{z,M} = 0.2$ . The specific flow states and parameters considered are WVF<sub>2</sub> (5V,  $k = 4.21$ ) at  $s_{z,S} = 0.2 = s_{z,M}$  and WVF<sub>2</sub> (4V,  $k = 3.69$ ) at  $s_{z,S} = 0.25, s_{z,M} = 0.2$ . The observations are qualitatively identical to those for smaller parameters  $s_{z,S} = 0.1 = s_{z,M}$ , with respect to variation in modes and frequencies according to the driving frequency  $\Omega_H$ . Similar delays and overshooting are detected, but they are more pronounced in general. Additionally, WVF<sub>2</sub> (5V,  $k = 4.21$ ) does not exist stable for pure static field and small driving frequency  $\Omega_H$ , and the system transitions toward another solution for driving frequencies  $\Omega_H \lesssim 0.57$ , which results in irregular intermittency (see later discussion in Sec. III E).

The latter illustrate a closed circle (in particular two circles) as manifestation for the two-torus characteristics. Within one period, the system spend extended time with retrograde  $\omega_{2,4,21} < 0$  (region A) and prograde dynamics  $\omega_{2,4,21} > 0$  (region B) [cf. Fig. 8(b)]. In fact, the time that the system spend with prograde and retrograde dynamics is almost identical. This is also visible in the corresponding  $(\eta_-, \eta_+)$  phase space trajectory [Fig. 8(c)], which looks like two loops with shape of an “eight” on top of each other (cf. small loops for small parameters  $s_{z,S} = 0.1 = s_{z,M}$  in Fig. 5 that indicated the short prograde dynamics).

The Poincaré section (at  $\eta_- = 500$ ) exhibits a closed circle (in particular two circles), manifesting the two-torus characteristics. Within one period, the system spends extended time with retrograde  $\omega_{2,4,21} < 0$  (region A) and prograde dynamics  $\omega_{2,4,21} > 0$  (region B) [cf. Fig. 8(b)]. The time spent with prograde and retrograde dynamics is almost identical, which is visible in the corresponding  $(\eta_-, \eta_+)$  phase space trajectory [Fig. 8(c)], resembling two loops with the shape of an “eight” on top of each other (cf. small loops for small parameters  $s_{z,S} = 0.1 = s_{z,M}$  in Fig. 5 indicating an only short prograde dynamics).

When the system operates under these parameters, it takes around four driving time periods  $T_H$  to approach the initial solution [Fig. 8(c)]. This is less than half the time compared to the scenario with smaller field parameters  $s_{z,S} = 0.2 = s_{z,M}$  [Fig. 5(1b)]. The flow pattern reversal for WVF<sub>2</sub> (5V,  $k = 4.21$ ) transitioning from retrograde ( $\omega < 0$ ) to prograde ( $\omega > 0$ ) and vice versa is illustrated in Fig. 9 [top row (multimedia online), middle row (multimedia online), and bottom row (multimedia online)] for different times  $t_i, i \in \{1; 4\}$  according to Fig. 8(b).

At times  $t_1$  and  $t_3$  (region A), the flow is retrograde, while it is prograde at times  $t_2$  and  $t_4$ . However, due to the non-linear, asymmetric effects of the magnetic field, the overall or average value  $\overline{\omega}_{2,4,21} = -2.15$  is negative, resulting in the overall flow dynamics remaining retrograde (Fig. 9, multimedia online).

For WVF<sub>2</sub> (4V,  $k = 3.69$ ) at the given magnetic field parameter  $s_{z,S} = 0.45, s_{z,M} = 0.2$ , the average frequency  $\overline{\omega}_{2,3,69}$  is positive but very close to zero [Fig. 3(1c)]. This results in the flow being retrograde and prograde almost an equal amount of time. However, the oscillation characteristics show that there is a small overall prograde dynamics remaining. This is due to the slightly positive mean frequency  $\overline{\omega}_{2,3,69} = 0.204$  (Fig. 11, multimedia online). The variations in kinetic energy  $E_{kin}$  and mode amplitudes  $|u_{m,k}|$  remain relatively straightforward, while the azimuthal vorticity  $\eta_\pm$  highlights the characteristics of a two-torus  $T_2$  solution [Fig. 10(c)]. It takes about six periods  $T_H$  for the solution to come close to the initial state [compared points 1 and 6 in Fig. 10(c)].

The flow visualizations for the temporal flow pattern reversal for WVF<sub>2</sub> (4V,  $k = 3.69$ ) illustrate the transition from retrograde ( $\omega < 0$ ) to prograde ( $\omega > 0$ ) and vice versa in Fig. 11 top row (multimedia online), middle row (multimedia online), and bottom row (multimedia online)]. These visualizations correspond to different times  $t_i, i \in \{1; 4\}$  according to Fig. 10(b). In region A at times  $t_1$  and  $t_3$ , the flow is retrograde, while at times  $t_2$  and  $t_4$ , it is prograde. The flow dynamics mainly consist of oscillations with almost identical times for retrograde and prograde dynamics. However, since the average value  $\overline{\omega}_{2,3,69} = 0.204$  is very small but positive, the flow exhibits an overall prograde dynamics.

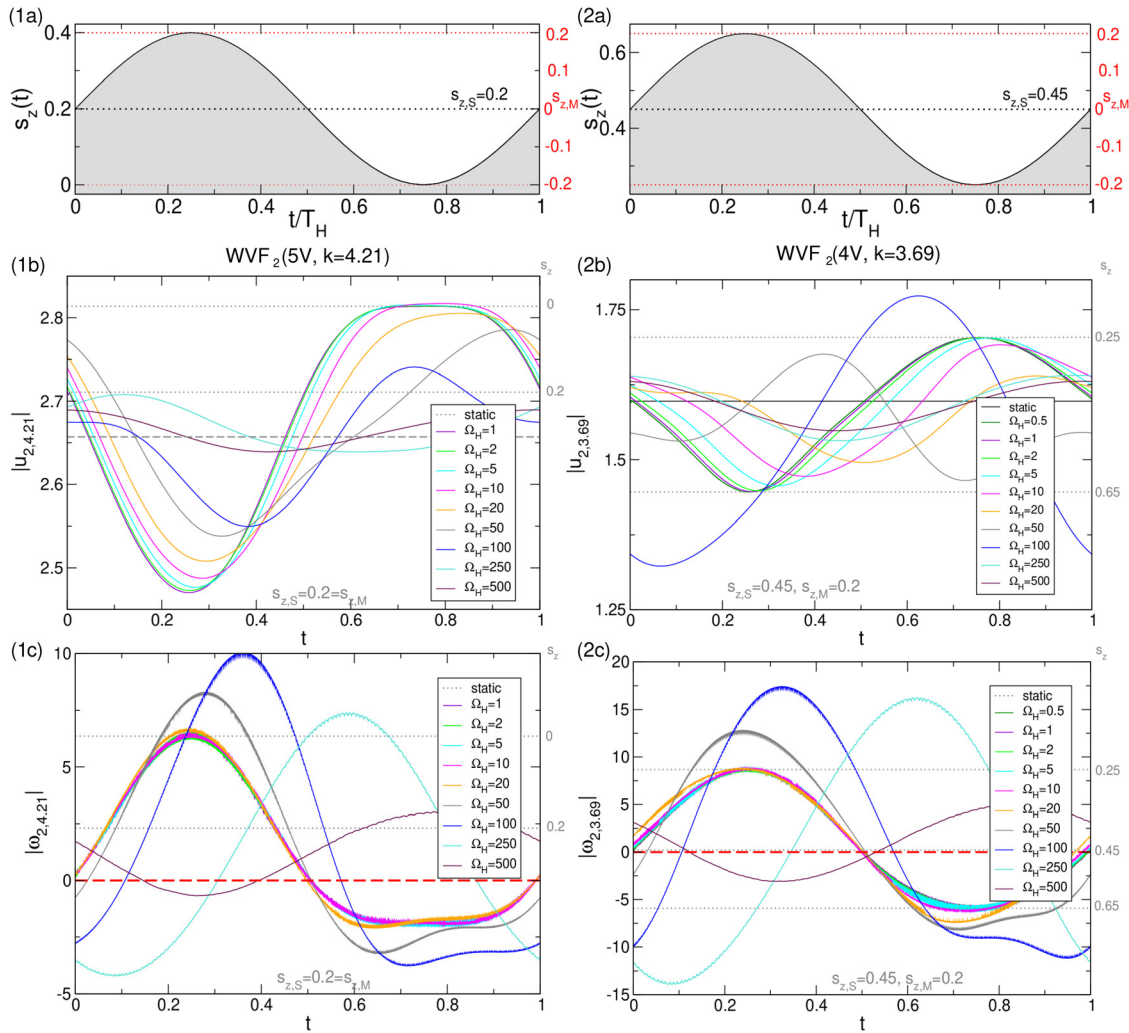


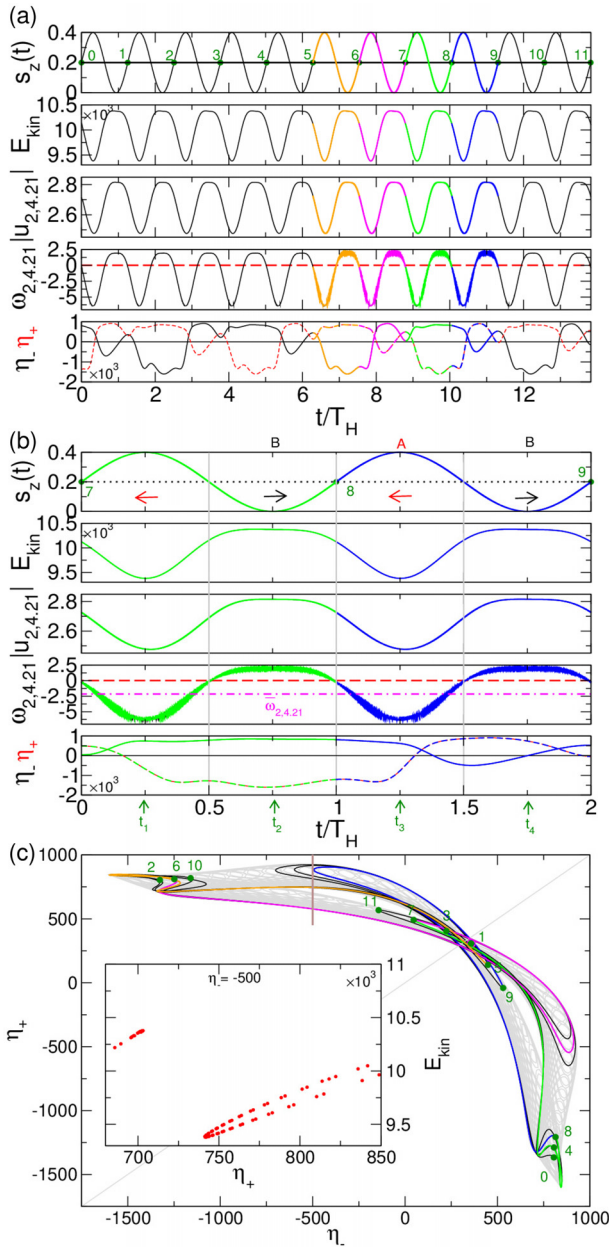
**FIG. 7.** As Fig. 4 for flow states (1)  $WVF_2(5V, k = 4.21)$  ( $|u_{2,4.21}|$  and  $|\omega_{2,4.21}|$ ) at control parameters  $s_{z,S} = 0.2 = s_{z,M}$  and (2)  $WVF_2(4V, k = 3.69)$  ( $|u_{2,3.69}|$  and  $|\omega_{2,3.69}|$ ) at control parameters  $s_{z,S} = 0.25, s_{z,M} = 0.2$ . Worth to point out that for frequencies  $\Omega_H \leq 0.57$ , the system shows irregular intermittency as  $WVF_2(5V, k = 4.21)$  loses its stability and the flow transitions to another solution. The latter is randomly selected and either  $WVF_2(4V, k = 3.85)$  or  $WVF_2(4V, k = 3.69)$ . See also later discussion and Sec. III E. Note, in (1b) and (1c) no curve for  $\Omega_H = 0.5$  as well no dotted lines for static field  $s_{z,S}$  are shown as here  $WVF_2(5V, k = 4.21)$  is unstable.

### E. Intermittency

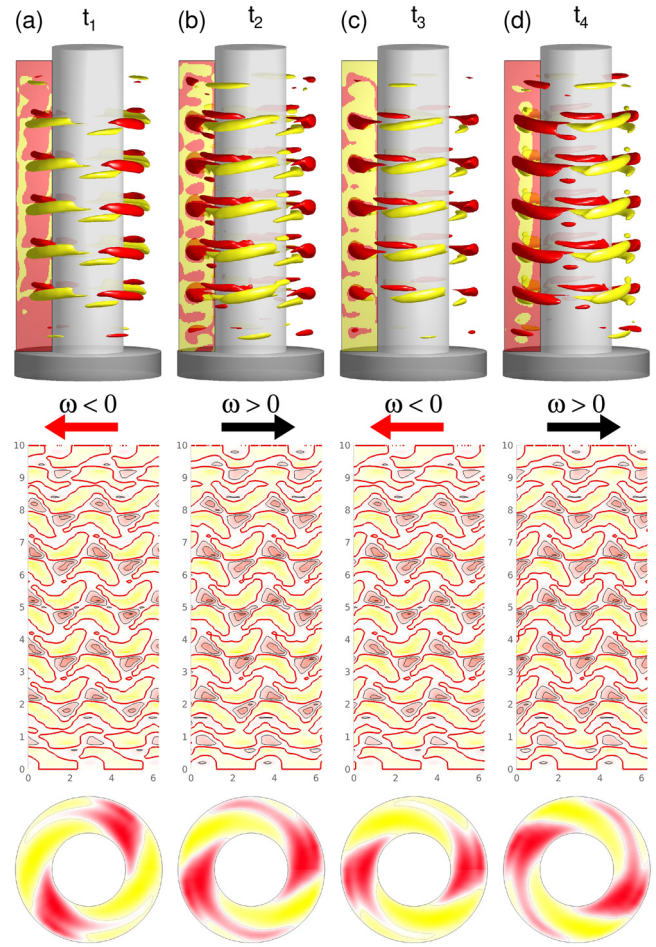
In Sec. IV, we will take a closer look at  $WVF_2(5V, k = 4.21)$  and analyze its behavior under an alternating magnetic field with  $s_{z,S} = 0.2 = s_{z,M}$  at frequencies  $\Omega_H \leq 0.57$ . As mentioned previously (see Fig. 8), the flow becomes unstable and transitions to another solution. During this process, intermittent dynamics are observed (see Fig. 12). The final solution to which the flow transitions may vary, and the intermittency time  $t_{inter}$  required for the system to reach the new solution is irregular. While Fig. 12(c) suggests a preference for a transition toward  $WVF_2(4V, k = 3.85)$  at lower frequencies  $\Omega_H$ , numerous long-time simulations did not reveal any correlation between the initial state  $WVF_2(5V, k = 4.21)$  and the final states  $WVF_2(4V, k = 3.85)$  or  $WVF_2(4V, k = 3.69)$ .

Figure 12 shows three examples of the transition toward  $WVF_2(5V, k = 3.85)$ ,  $WVF_2(5V, k = 3.69)$ , and  $WVF_2(4V, k = 3.61)$ ,

respectively, along with the transition/intermittency time  $t_{inter}$  for various  $\Omega_H$ . It is worth noting that the coexistence with other wavy vortex flows with a larger azimuthal wave number  $m = 3$ , specifically  $WVF_3(4V, k = 3.61)$ , at the given parameters is not uncommon. However, as it is not pertinent to the present study, we refer to the discussion in our earlier work.<sup>40</sup> In general, it seems that when the transition occurs toward  $WVF_2(5V, k = 3.69)$ , the average intermittency time  $\bar{t}_{inter}(5V, k = 4.21) \rightarrow (5V, k = 3.69)$  is greater than the corresponding intermittency time  $\bar{t}_{inter}(5V, k = 4.21) \rightarrow (5V, k = 3.85)$  when the transition goes toward  $WVF_2(5V, k = 3.85)$  [see horizontal dashed lines in Fig. 12(c)]. Also, for small but increasing  $\Omega_H$ , there seems to be a similar tendency in increasing time  $\bar{t}_{inter}(5V, k = 4.21) \rightarrow (5V, k = 3.85)$ . On the other hand, no correlation appears to exist between  $\Omega_H$  and the time  $\bar{t}_{inter}(5V, k = 4.21) \rightarrow (5V, k = 3.85)$ . Although there is no defined intermittent time, it



**FIG. 8.** Flow dynamics evolving with time  $t$  for  $WV_2$  ( $5V, k = 4.21$ ) for an alternating magnetic field with  $s_{z,S} = 0.2 = s_{z,M}$  and  $\Omega_H = 5$ , shown are: (a) variation with time of the magnetic field  $s_z(t)$ , the modal kinetic energy  $E_{kin}$  [Eq. (6)], moduli  $|u_{m,k}|$  of the dominant axial Fourier amplitudes of the azimuthal modes  $u_m(z, t)$  [Eq. (5)] of the radial flow at mid-gap, the corresponding frequencies  $\omega_{m,k}$  and the vorticity  $\eta_{-/+} = \eta(r = r_i, \theta = 0, z = \Gamma/4[3\Gamma/4])$ . (b) Close up of (a) covering two periods. Small arrows below the abscissa indicate time steps  $t_i, i \in \{1; 4\}$  for which snapshots are shown in Fig. 9. Red dashed line indicates  $\omega_{2,4,21} = 0$ , while magenta dot-dashed line indicates the mean value  $\bar{\omega}_{2,4,21} = -2.15$ . (c) Phase portraits in  $(\eta_-, \eta_+) = (\eta(r = r_i, \theta = 0, z = \Gamma/4), \eta(r = r_i, \theta = 0, z = 3\Gamma/4))$  plane; the inset shows the Poincaré section for  $\eta_- = -500$  (see vertical brown line). Each oscillation period  $T_H$  is coded by a different color and the same color code is used for each subplot. The gray colored line in (c) indicates the diagonal  $\eta_+ = \eta_-$ .



**FIG. 9.** Flow visualizations of the temporal flow pattern reversal for  $WV_2$  ( $5V, k = 4.21$ ) with  $s_{z,S} = 0.2 = s_{z,M}$  and  $\Omega_H = 5$  for retrograde ( $\omega < 0$ ) and prograde ( $\omega > 0$ ) situations at times  $t_i, i \in \{1; 4\}$  as indicated in Fig. 5(c). Top row: isosurfaces of azimuthal vorticity  $\eta = \pm 200$  [red (yellow) color indicates positive (negative) vorticity]. Middle row: radial velocity  $u(\theta, z)$  on an unrolled cylindrical surface in the annulus at mid-gap [red (yellow) color indicates in (out) flow]. Bottom row: contours of azimuthal velocity component  $v$  in the  $(r, \theta)$  plane at mid-height (viewed from the bottom) [red (yellow) color indicates positive (negative) velocity]. Multimedia files show two periods,  $T_\Omega \approx 1.257$ , of the alternating field. Multimedia available online.

seems that for a set of system parameters, there is an upper time limit for the transition. In our case, we observed the intermittency time to always be smaller than two periods of the alternating magnetic field  $T_\Omega$ . To provide a better understanding of the flow dynamics, the transitions for selected parameters together with corresponding phase space trajectories are illustrated in Figs. 12(1)–12(3). It is important to note that here all solutions are  $T_2$  and the corresponding curves are just small segments of the complete solution. Meanwhile, points with dotted lines illustrate the departure and arrival from any of the solutions, while gray dots indicate the intermittent behavior.

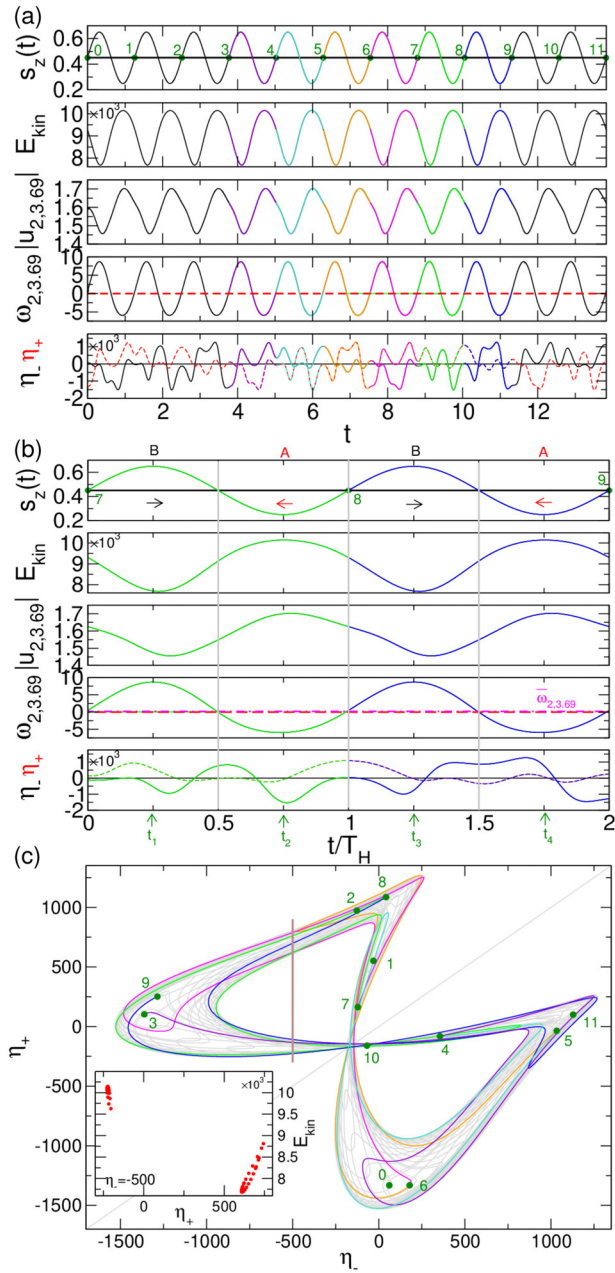


**FIG. 10.** Flow dynamics evolving with time  $t$  for  $WVF_2$  ( $4V, k = 3.69$ ) for an alternating magnetic field with  $s_{z,S} = 0.45$ ,  $s_{z,M} = 0.2$ , and  $\Omega_H = 5$ ; shown are: (a) variation with time of the magnetic field  $s_z(t)$ , the modal kinetic energy  $E_{kin}$  [Eq. (6)], moduli  $|u_{m,k}|$  of the dominant axial Fourier amplitudes of the azimuthal modes  $u_m(z, t)$  [Eq. (5)] of the radial flow at mid-gap, the corresponding frequencies  $\omega_{m,k}$  and the vorticity  $\eta_{-/+} = \eta(r = r_i, \theta = 0, z = \Gamma/4[3\Gamma/4])$ . (b) Close up of (a) covering two periods. Small arrows below the abscissa indicate time steps  $t_i, i \in \{1; 4\}$  for which snapshots are shown in Fig. 9. Red dashed line indicates  $\omega_{2,3,69} = 0$ , while magenta dot-dashed line indicates the mean value  $\overline{\omega_{2,3,69}} = 0.204$ , which are almost indistinguishable in the figure. (c) Phase portraits in  $(\eta_-, \eta_+) = (\eta(r = r_i, \theta = 0, z = \Gamma/4), \eta(r = r_i, \theta = 0, z = 3\Gamma/4))$  plane; the inset shows the Poincaré section for  $\eta_- = -500$  (see vertical brown line). The gray colored line in (c) indicates the diagonal  $\eta_+ = \eta_-$ .

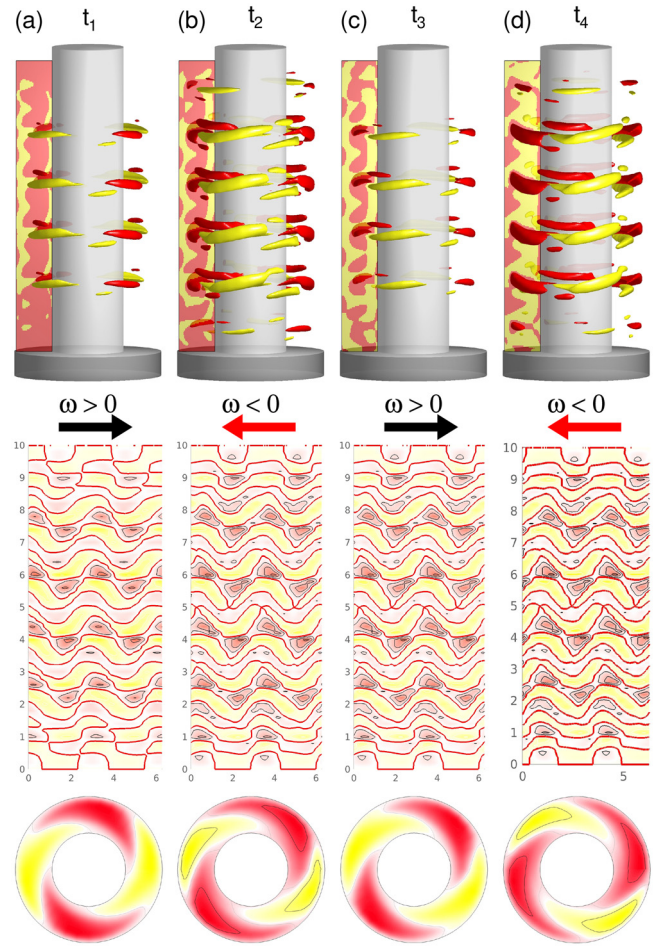


**FIG. 11.** Temporal flow pattern reversal for  $WVF_2$  ( $4V, k = 3.69$ ) with  $s_{z,S} = 0.45$ ,  $s_{z,M} = 0.2$ , and  $\Omega_H = 5$  for retrograde ( $\omega < 0$ ) and prograde ( $\omega > 0$ ) situations at times  $t_i, i \in \{1; 4\}$  as indicated in Fig. 10. Top row: isosurfaces of azimuthal vorticity  $\eta = \pm 200$  [red (yellow) color indicates positive (negative) vorticity]. Middle row: radial velocity  $u(\theta, z)$  on an unrolled cylindrical surface in the annulus at mid-gap [red (yellow) color indicates in (out) flow]. Bottom row: contours of azimuthal velocity component  $v$  in the  $(r, \theta)$  plane at mid-height (viewed from the bottom) [red (yellow) color indicates positive (negative) velocity]. Multimedia files show two periods,  $T_\Omega \approx 1.257$ , of the alternating field. Multimedia available online.

#### IV. CONCLUSIONS

We have discovered that under an applied external magnetic field in a wide gap, finite length,  $\Gamma = 10$ , Taylor–Couette system between counter-rotating cylinders, there can be a reversal in the way waves propagate for supercritical twofold symmetric wavy vortex flow ( $WVF_2$ ) with dominant  $m = 2$  azimuthal wave number. Even though different  $WVF_2$  have the same  $m = 2$  azimuthal wave number, we observed that they can have different numbers of vortex pairs ( $4V$  and  $5V$ ) within the annulus and different axial wavenumbers. The axial wavenumbers for  $5V$  are  $k = 4.21$ , and for  $4V$ , they are  $k = 3.85$  and  $k = 3.69$ . Depending on other system parameters, these solutions can be stable or unstable.

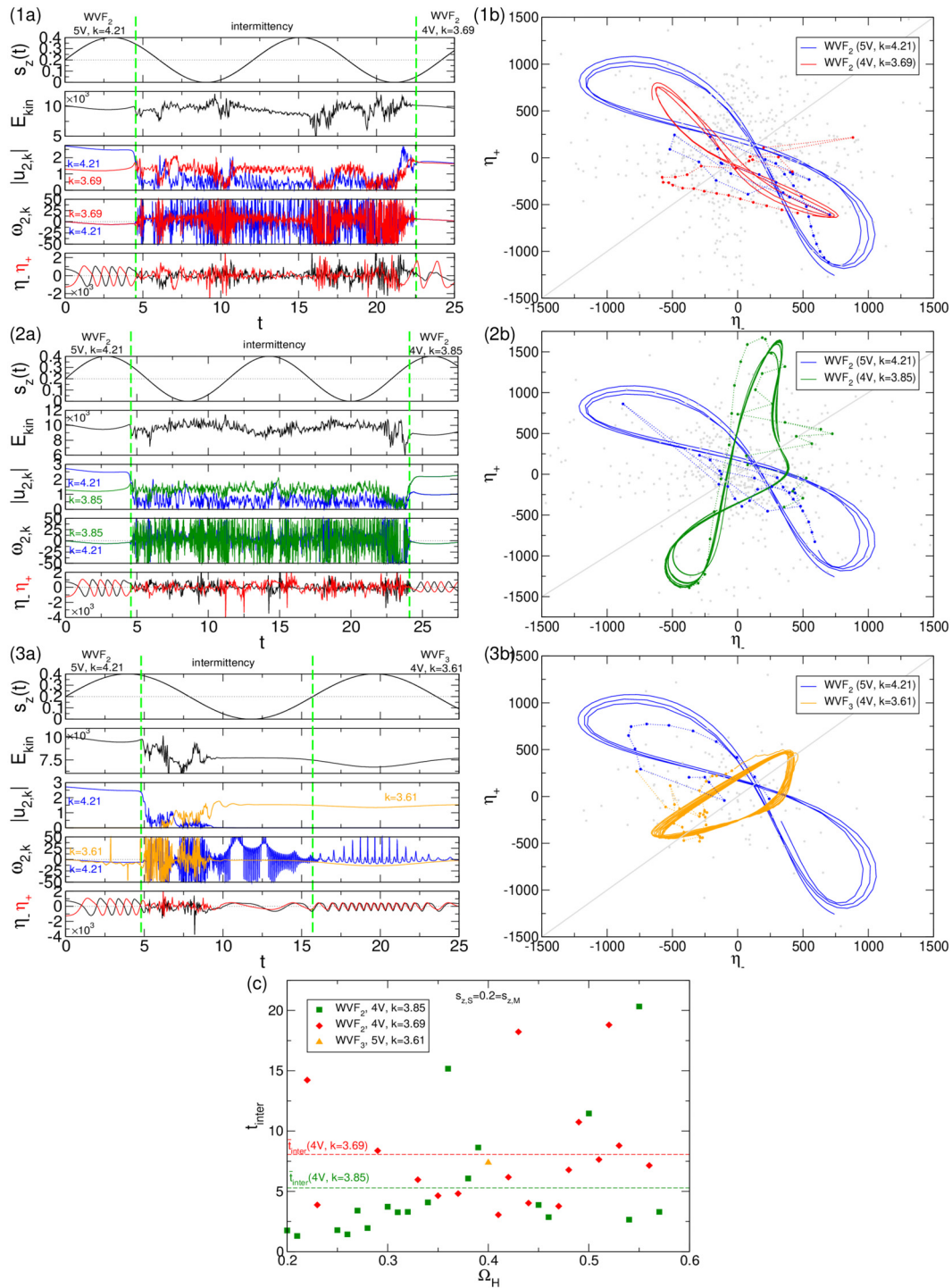


**FIG. 12.** Flow dynamics evolving with time  $t$  under alternating magnetic field with  $s_{z,S} = 0.2 = s_{z,M}$  when intermittency appears. Initial state  $WVF_2$  (5V,  $k = 4.21$ ) with transition toward (1)  $WVF_2$  (4V,  $k = 3.69$ ) at  $\Omega_H = 0.52$ , (2)  $WVF_2$  (4V,  $k = 3.85$ ) at  $\Omega_H = 0.55$ , and (3)  $WVF_3$  (4V,  $k = 3.61$ ) at  $\Omega_H = 0.4$ . (a) Variation with time of the magnetic field  $s_z(t)$ , the modal kinetic energy  $E_{kin}$  [Eq. (6)], moduli  $|u_{m,k}|$  of the dominant axial Fourier amplitudes of the azimuthal modes  $u_m(z, t)$  [Eq. (5)] of the radial flow at mid-gap, the corresponding frequencies  $\omega_{m,k}$  and the vorticity  $\eta_{-+} = \eta(r = r_1, \theta = 0, z = \Gamma/4[3\Gamma/4])$ . (b) Corresponding phase portraits in  $(\eta_-, \eta_+)$  plane illustrating the transition. Intermittency while transition from  $WVF_2$  (5V,  $k = 4.21$ ) toward top:  $WVF_2$  (4V,  $k = 3.69$ ) at  $\Omega_H = 0.52$  and middle:  $WVF_2$  (4V,  $k = 4.85$ ) at  $\Omega_H = 0.55$ . Note, only fragments of the different  $T_2$  solutions  $WVF_2$  and  $WVF_3$  are shown. (c) Intermittent time  $t_{inter}$  vs driving frequency  $\Omega_H$  during the random transitions.

We have studied wave propagation reversal for both static and alternating magnetic fields. In the absence of a magnetic field, the  $WVF_2$  moves in a retrograde manner relative to the inner cylinder rotation. However, when we increase the strength of a static or alternating magnetic field, the retrograde wave propagation slows down and eventually becomes zero. At this point, the flow is represented by a *standing wave* and then starts moving in the opposite direction, becoming prograde. The reversal of wave propagation coincides with the stabilization of the basic state due to increasing magnetic field strength, both for static and alternating fields.<sup>24,27</sup> With an axial magnetic field, we noticed at most one reversal. However, it is important to note that scenarios with a second reversal have been reported under a symmetry-breaking transverse magnetic field,<sup>24,35</sup> and even in the absence of any external forcing.<sup>40</sup>

When analyzing the response of the system to different flow states of  $WVF_2$ , we noticed that as the oscillation frequency  $\Omega_H$  increases, the system's temporal evolution decreases. In general, at high frequencies, only the average of the externally applied magnetic field influences the system, as the fluid's inertia cannot keep up with rapid changes in acceleration caused by the Kelvin force. The stability boundary for an alternating magnetic field at high frequencies corresponds to a static stability boundary, which is above the mean of the alternating magnetic field. This happens because during one modulation period, the system experiences a stronger stabilization effect when the modulation amplitude is above the average field strength, compared to the destabilization in the other half-period.

For low frequency, the static scenario is most likely approached. In addition, we also observed intermittent behavior when one solution becomes unstable for low frequencies. Therefore, the transition appears random in two ways: either in time or toward different final solutions. However, a maximum persistence time predetermined by the system parameters can be identified, which is about two periods of driving, but further investigations are necessary to fully understand this behavior.

The present work indicates the impact of complex fluids under external driving forces. As such, the variation in frequency of the alternating field provides a very simple and, in particular, accurate controllable way to trigger the system response of the flow to be prograde or retrograde.

In future works involving alternating magnetic fields, it would be beneficial to focus on analyzing wavy vortices with larger azimuthal wavenumbers ( $\geq 3$ ) and other complex structures of modulated rotating waves, such as mixed ribbons and mixed-cross spirals. The experimental system configuration and parameters discussed in this paper are easily accessible.<sup>31</sup> Therefore, experiments should be conducted to provide a comparison with the numerical results presented here. It is expected that the experimental and numerical results will be in good agreement, especially for the onset of nonlinear instabilities under static magnetic fields. The recent experimental study by Ilzig *et al.*<sup>44</sup> raises an intriguing question about the behavior of flow structures when an alternating magnetic field is applied instead of a static one.

## ACKNOWLEDGMENTS

S.A. is a Serra Hünter Fellow. This work has been supported by the Spanish Government under Grant No. PID2019-105162RB-I00.

## AUTHOR DECLARATIONS

### Conflict of Interest

The authors have no conflicts to disclose.

### Author Contributions

**Sebastian A. Altmeyer:** Conceptualization (equal); Data curation (equal); Formal analysis (equal); Investigation (equal); Methodology (equal); Project administration (equal); Resources (equal); Software (equal); Validation (equal); Visualization (equal); Writing – original draft (equal); Writing – review & editing (equal).

### DATA AVAILABILITY

The data that support the findings of this study are available from the corresponding author upon reasonable request.

## REFERENCES

- 1A. Cox, *Plate Tectonics and Geomagnetic Reversal* (W. H. Freeman Publishers, San Francisco, CA, 1973), pp. 138–145, 222–228.
- 2G. A. Glatzmaier and P. H. Roberts, “A three dimensional self-consistent computer simulation of a geomagnetic field reversal,” *Nature* **377**, 203–209 (1995).
- 3G. A. Glatzmaier, R. S. Coe, L. Hongre, and P. H. Roberts, “The role of the earth’s mantle in controlling the frequency of geomagnetic reversals,” *Nature* **401**, 885–890 (1999).
- 4G. A. Glatzmaier and P. H. Roberts, “Geodynamo theory and simulations,” *Rev. Mod. Phys.* **72**, 1081–1123 (2000).
- 5M. Berhanu *et al.*, “Magnetic field reversals in an experimental turbulent dynamo,” *Europhys. Lett.* **77**, 59001 (2007).
- 6G. I. Taylor, “Stability of a viscous liquid contained between two rotating cylinders,” *Philos. Trans. R. Soc. London A* **223**, 289 (1923).
- 7P. Chossat and G. Iooss, *The Couette–Taylor Problem* (Springer, Berlin, 1994).
- 8R. C. DiPrima, “The stability of a viscous fluid between rotating cylinders with an axial flow,” *J. Fluid Mech.* **9**, 621 (1960).
- 9S. Chandrasekhar, *Hydrodynamic and Hydromagnetic Stability* (Dover, New York, 1961).
- 10C. D. Andereck, S. S. Liu, and H. L. Swinney, “Flow regimes in a circular Couette system with independently rotating cylinders,” *J. Fluid Mech.* **164**, 155–183 (1986).
- 11R. Donnelly, “Taylor-Couette flow: The early days,” *Phys. Today* **44**(11), 32 (1991).
- 12H. Kuhlmann, D. Roth, and M. Lücke, “Taylor vortex flow under harmonic modulation of the driving force,” *Phys. Rev. A* **39**, 745 (1989).
- 13B. T. Murray, G. B. McFadden, and S. R. Coriell, “Stabilization of Taylor–Couette flow due to time-periodic outer cylinder oscillation,” *Phys. Fluids A Fluid Dyn.* **2**, 2147 (1990).
- 14F. Marques and J. M. Lopez, “Taylor-Couette flow with axial oscillations of the inner cylinder: Floquet analysis of the basic flow,” *J. Fluid Mech.* **348**, 153 (1997).
- 15C. Normand, “Stability of time-periodic flows in a Taylor–Couette geometry,” *Phys. Rotat. Fluids* **549**, 67 (2000).
- 16M. Sinha, I. G. Kevrekidis, and A. J. Smiths, “Experimental study of a Neimark–Sacker bifurcation in axially forced Taylor–Couette flow,” *J. Fluid Mech.* **558**, 1 (2006).
- 17R. A. Verschoof, A. K. te Nijenhuis, S. G. Huisman, C. Sun, and D. Lohse, “Periodically driven Taylor–Couette turbulence,” *J. Fluid Mech.* **846**, 834 (2018).
- 18R. E. Rosensweig, *Ferrohydrodynamics* (Cambridge University Press, Cambridge, 1985).
- 19J. E. Hart, “Ferromagnetic rotating Couette flow: The role of magnetic viscosity,” *J. Fluid Mech.* **453**, 21–38 (2002).
- 20J. E. Hart and S. Kittelman, “A magnetic fluid laboratory model of the global buoyancy and wind-driven ocean circulation: Experiments,” *Dyn. Atmos. Oceans* **41**, 139–147 (2006).

- <sup>21</sup>S. Sütterlin *et al.*, “Fargo: Validation of space-relevant ferrofluid applications on the ISS,” *CEAS Space J.* **16**, 731 (2024).
- <sup>22</sup>S. Zajonz *et al.*, “Development of a ferrofluid-based attitude control actuator for verification on the ISS,” *Aerotec. Missili Spaz.* **103**, 303–314 (2024).
- <sup>23</sup>M. Niklas, “Influence of magnetic fields on Taylor vortex formation in magnetic fluids,” *Z. Phys. B: Condens. Matter* **68**, 493 (1987).
- <sup>24</sup>S. Altmeyer, C. Hoffmann, A. Leschhorn, and M. Lücke, “Influence of homogeneous magnetic fields on the flow of a ferrofluid in the Taylor-Couette system,” *Phys. Rev. E* **82**, 016321 (2010).
- <sup>25</sup>M. Reindl and S. Odenbach, “Influence of a homogeneous axial magnetic field on Taylor-Couette flow of ferrofluids with low particle-particle interaction,” *Exp. Fluids* **50**, 375 (2011).
- <sup>26</sup>S. Altmeyer, “Ferrofluidic Couette flow in time-varying magnetic field,” *J. Magn. Magn. Mater.* **552**, 169205 (2022).
- <sup>27</sup>S. Altmeyer, “On the ridge of instability in ferrofluidic Couette flow via alternating magnetic field,” *Sci. Rep.* **11**, 4705 (2021).
- <sup>28</sup>S. A. Altmeyer, “Ferrofluidic wavy Taylor vortices under alternating magnetic field,” *Philos. Trans. R. Soc. A* **381**, 20220121 (2023).
- <sup>29</sup>S. Altmeyer, “Increasing flow complexity in time-dependent modulated ferrofluidic Couette flow,” *Fluid Dyn.* **57**(3), 387 (2022).
- <sup>30</sup>S. Altmeyer, J. Lopez, and Y. Do, “Effect of elongational flow on ferrofluids under a magnetic field,” *Phys. Rev. E* **88**, 013003 (2013).
- <sup>31</sup>M. Reindl and S. Odenbach, “Effect of axial and transverse magnetic fields on the flow behavior of ferrofluids featuring different levels of interparticle interaction,” *Phys. Fluids* **23**, 093102 (2011).
- <sup>32</sup>C. Hoffmann, S. Altmeyer, A. Pinter, and M. Lücke, “Transitions between Taylor vortices and spirals via wavy Taylor vortices and wavy spirals,” *New J. Phys.* **11**, 053002 (2009).
- <sup>33</sup>J. Embs, H. W. Müller, C. Wagner, K. Knorr, and M. Lücke, “Measuring the rotational viscosity of ferrofluids without shear flow,” *Phys. Rev. E* **61**, R2196 (2000).
- <sup>34</sup>The specifications for the ferrofluid APG933 are as follows:  $\mu_0 M_s = 20$  mT,  $\eta = 500$  mPa s, density  $\rho = 1.09$  g/cm<sup>3</sup>,  $\Phi_m = 3.3\%$ , susceptibility  $\chi = 0.9$ , mean diameter of the particle’s magnetic core 10 nm, and thickness of the polymeric coating 2 nm.
- <sup>35</sup>S. Altmeyer, Y. Do, and Y.-C. Lai, “Magnetic field induced flow pattern reversal in a ferrofluidic Taylor-Couette system,” *Sci. Rep.* **5**, 18589 (2015).
- <sup>36</sup>H. W. Müller and M. Liu, “Structure of ferrofluid dynamics,” *Phys. Rev. E* **64**, 061405 (2001).
- <sup>37</sup>S. Hughes and A. Randriamampianina, “An improved projection scheme applied to pseudospectral methods for the incompressible Navier Stokes equations,” *Int. J. Numer. Meth. Fluids* **28**, 501 (1998).
- <sup>38</sup>I. Mercader, O. Batiste, and A. Alonso, “An efficient spectral code for incompressible flows in cylindrical geometries,” *Comput. Fluids* **39**, 215 (2010).
- <sup>39</sup>S. Altmeyer, C. Hoffmann, M. Heise, J. Abshagen, A. Pinter, M. Lücke, and G. Pfister, “End wall effects on the transitions between Taylor vortices and spiral vortices,” *Phys. Rev. E* **81**, 066313 (2010).
- <sup>40</sup>S. Altmeyer and R. Lueptow, “Wave propagation reversal for wavy vortices in wide-gap counter-rotating cylindrical Couette flow,” *Phys. Rev. E* **95**, 053103 (2017).
- <sup>41</sup>M. I. Shliomis and K. I. Morozov, “Negative viscosity of ferrofluid under alternating magnetic field,” *Phys. Fluids* **6**, 2855 (1994).
- <sup>42</sup>R. Rosensweig, “Heating magnetic fluid with alternating magnetic field,” *J. Magn. Magn. Mater.* **252**, 370 (2002).
- <sup>43</sup>M. Goharkhah, A. Salarian, M. Ashjaee, and M. Shahabadi, “Convective heat transfer characteristics of magnetite nanofluid under the influence of constant and alternating magnetic field,” *Powder Technol.* **274**, 258 (2015).
- <sup>44</sup>T. Ilzig, K. Stöckel, and S. Odenbach, “Experimental investigations on the effect of axial homogeneous magnetic fields on propagating vortex flow in the Taylor-Couette system,” *Materials*. **12**, 4027 (2019).